Chemical Geology 431 (2016) 44–53

Contents lists available at ScienceDirect

Chemical Geology

journal homepage: www.elsevier.com/locate/chemgeo

Carbon speciation in saline solutions in equilibrium with aragonite at high pressure

Sébastien Facq [a,1], Isabelle Daniel [a,*], Gilles Montagnac [a], Hervé Cardon [a], Dimitri A. Sverjensky [b]

[a] Univ Lyon, Univ Lyon 1, Ens de Lyon, CNRS, UMR 5276 Laboratoire de Géologie de Lyon, F-69622, Villeurbanne, France
[b] Dept. Earth & Planetary Sciences, Johns Hopkins University, 3400 N. Charles St., Baltimore, MD 21218, USA

ARTICLE INFO

Article history:
Received 17 September 2015
Received in revised form 16 March 2016
Accepted 17 March 2016
Available online 28 March 2016

Keywords:
Carbonates
Deep fluids
In situ Raman spectroscopy
Diamond anvil cell experiments
Deep Earth Water model

ABSTRACT

The solubility of carbonate minerals and aqueous carbonate speciation in deep fluids is of critical importance to the long-term carbon cycle. However, no experimental data exist in the calcium carbonate–water–salt system at pressures greater than 10 kbar. Here we present an integrated experimental and theoretical study of carbon speciation and solubility during equilibration of aragonite with NaCl solutions at 300 °C from 20 to 70 kbar. Using *in situ* Raman spectroscopy in a diamond anvil cell with NaCl concentrations up to 1.0 *m* (5.5 wt.%), bicarbonate and carbonate ions were the only C-bearing aqueous species spectroscopically detected in the fluids. The proportion of total dissolved bicarbonate to carbonate increased with NaCl concentration and was interpreted using a thermodynamic model to retrieve the dissociation constant of the $NaHCO_3^0$ complex. The results were extended to higher temperatures using the Deep Earth Water (DEW) model to predict calcite solubility and speciation at 700 °C and 10 kbar in chloride solutions. With a one parameter extension of the Debye–Hückel model, the calculated solubilities agree with data from Newton and Manning (2002) up to 10 *m* NaCl where the solubility is about 250 millimolal. Such solubilities might contribute substantial transport of carbon in fluids at depth in subduction zones.

1. Introduction

The mass balance of carbon between the subduction of carbon-bearing oceanic lithosphere into the Earth's mantle and the return of CO_2 to the atmosphere by volcanic and metamorphic degassing is critical to the maintenance of a steady state of the global carbon cycle on geologic timescales (Berner, 2004). The latest estimates indicate that 4–8.8 × 10^{13} g of C $year^{-1}$ enter subduction zones globally (Dasgupta, 2013; Kelemen and Manning, 2015), mostly as carbonate minerals in metasedimentary rocks, and that the global arc flux of CO_2 is 1.8–4.3 × 10^{13} g of C $year^{-1}$ (Sano and Williams, 1996; Kelemen and Manning, 2015). This implies that up to 100% of the original carbon input to subduction zones may be returned to the atmosphere by arc magmatism. In contrast, petrologic prediction of metamorphic decarbonation has indicated limited devolatilization of CO_2, implying preservation of carbonate in subducting slabs deep into the Earth (*e.g.*, Yaxley and Green, 1994; Kerrick and Connolly, 1998, 2001a,b; Molina and Poli, 2000; Hacker et al., 2003a,b; Dasgupta et al., 2005; van Keken et al., 2011; Tsuno and Dasgupta, 2012).

Within the last couple of years, field and analytical studies of subducted high-pressure rocks have revealed that carbonate minerals such as calcite or aragonite may have undergone substantial dissolution in the aqueous fluids released by the numerous dehydration reactions that occur during subduction. For instance, fluid inclusions in garnet in ultrahigh-pressure subducted rocks can contain a range of dissolved silicate and carbonate species including large amounts of aqueous carbonate and bicarbonate ions, as well as carbonate crystals (Frezzotti et al., 2011). Another recent example on a larger scale is that of the high-pressure marbles of the Cycladic subduction complex, which may have lost between 60 and 90% of their initial carbonate content, originally in the form of calcite and aragonite (Ague and Nicolescu, 2014). However, the dissolution and speciation of such large amounts of calcium carbonate in deep aqueous fluids at pressures in excess of 20 kbar at temperatures of 500–600 °C have not been studied experimentally.

Extensive experimental and theoretical efforts have been made to understand aqueous carbonate ion speciation (Frantz, 1998; Martinez et al., 2004; Facq et al., 2014; Schmidt, 2014) and the solubilities of carbonate minerals (mainly calcite) in pure water or mixed solvents at high pressures and temperatures (Walther & Long, 1986; Fein & Walther, 1987, 1989; Newton & Manning, 2002; Caciagli & Manning, 2003; Sanchez-Valle et al., 2003; Newton & Manning, 2005; Duan & Li, 2008; Facq et al., 2014). These studies have shown that the solubilities

* Corresponding author at: Université Lyon 1, bât. Géode - 2 rue Raphael Dubois, F-69622 Villeurbanne cedex, France.
E-mail address: Isabelle.Daniel@univ-lyon1.fr (I. Daniel).
[1] Now at: Department of Earth Sciences, University of Cambridge, Downing Street, Cambridge CB2 3EQ, UK.

http://dx.doi.org/10.1016/j.chemgeo.2016.03.021
0009-2541/

of calcite and aragonite are greatly enhanced by pressure and that dissolved carbonate ions tend to predominate over bicarbonate ions at constant temperature as pressure increases.

The solubilities of calcite and aragonite in natural deep fluids in subduction zones are likely to be affected by a number of variables including oxygen fugacity, acidity, and salinity (Manning et al., 2013; Manning, 2014). For example, under oxidizing conditions, the carbon solubility and speciation can be expected to be strongly affected by the pH imposed by the mineral assemblages in contact with the fluids (Manning et al., 2013): in carbonate-rich metasedimentary rocks, the pH values in the fluids will be very different to those imposed by a carbonate + silicate mineral assemblage, yet no experimental studies of these differences exist for high pressures. Similarly, although the effect of NaCl on calcite solubility has been studied at pressures up to 2 kbar (Ellis, 1963; Malinin and Kanukov, 1971; Fein and Walther, 1989) and at 10 kbar (Newton and Manning, 2002), where the solubility is enormously enhanced up to *ca.* 3–3.5 mol kg^{-1} $CaCO_3$ close to halite saturation, no studies at higher pressures exist. Natural NaCl brines are well known in the fluid inclusions of shallow hydrothermal ore deposits and have also been reported in fluid inclusions inside eclogitic minerals formed during alpine subduction (*e.g.* Scambelluri and Philippot, 2001). Overall, our understanding of Ca-carbonate mineral solubilities and aqueous speciation in subduction zone fluids is seriously hampered by the lack of experimental data referring to high pressures, dissolved NaCl, and the presence of silicate mineral assemblages.

In a previous study (Facq et al., 2014), we presented the first experimental data for aqueous carbon speciation at pressures of 20–80 kbar in water in equilibrium with calcium carbonate. In this study, we present complementary data for aqueous carbon speciation in NaCl aqueous solutions. This is a critical step for two reasons. First, the addition of NaCl requires consideration of at least seven additional aqueous Na- and Cl-complexes in the fluids (see below). Second, the addition of Na-species, together with previously calibrated aqueous Al- and Si-species (Sverjensky et al., 2014), will, in future studies, enable prediction of theoretical models of Ca-carbonate solubility and C-speciation in the much broader chemical system Na_2O–CaO–Al_2O_3–SiO_2–H_2O–HCl, where there is not yet any experimental data at subduction-zone pressures.

In the experimental part of the present study, the bicarbonate and carbonate speciation was obtained by *in situ* Raman spectroscopy of 0.5 and 1.0 *m* NaCl solutions in equilibrium with aragonite at pressures up to 70 kbar at 300 °C. The results were compared to our previous results obtained in pure water over a similar range of pressures and temperatures (Facq et al., 2014). Experimentally-derived trends in the proportion of bicarbonate to carbonate ions with salinity were used to constrain a theoretical thermodynamic model of the experimental data by using equilibrium constants calculated with the DEW model (Sverjensky et al., 2014) to retrieve new equilibrium constants for the $NaHCO_3^0$ complex. These results were extrapolated to higher temperatures to predict the solubility of calcite in saline deep fluids for comparison with experimental solubilities.

2. Experimental and theoretical approaches

2.1. Experimental methods

Experiments were conducted in a membrane-type diamond anvil cell (DAC) designed for microspectroscopy (Chervin et al., 1995) and equipped with synthetic IIa diamond anvils of 500 μm culet diameters. A resistive coil surrounding the cell allowed heating the sample. Temperature was controlled by a K-type thermocouple attached with ceramic glue to one anvil as close as possible to the culet. Pressure inside the compression chamber was calculated from the *PT* calibrated shift of the carbonate ν_1 symmetric stretching mode of the aragonite crystal (Facq et al., 2014).

A fragment of a natural single crystal of calcite from Durango, Colorado (Caciagli and Manning, 2003) was loaded in a pre-indented rhenium gasket with either ultrapure H_2O (18 MΩ·cm) or saline aqueous solutions with 0.55 *m* or 1.0 *m* NaCl. Initially, the DAC was closed and the temperature was increased to 300 °C. Raman spectra were collected as a function of pressure along an isothermal path between 800 and 1300 cm^{-1} using a confocal Labram HR800 Raman spectrometer (Horiba Jobin-Yvon™) of 800 mm focal length, with a holographic grating of 1800 $g \cdot mm^{-1}$ coupled to a cooled Peltier front-illuminated CCD detector (1024 × 256 pixels). This configuration enabled a very high spectral resolution of 0.3 cm^{-1}. The excitation line at 514.5 nm was produced by an Ar^+ laser source (Spectra Physics™) focused on the sample using a Mitutoyo™ 50× long-working distance objective (0.42 N.A.). Laser power at the sample was 10 mW. Spectra were corrected from a linear baseline and peak characteristics were obtained by fitting Voigt profiles to the Raman bands using the commercial software Peakfit™. The relative amounts of the carbonate and bicarbonate ions were estimated from the relative areas of the respective Raman bands, after correction from their Raman cross-section as proposed by Frantz (1998).

2.2. Theoretical methods

The thermodynamic model of fluid speciation and the solubility of aragonite used in this study is identical to that published previously for aragonite in water (Facq et al., 2014), with the additional consideration of equilibria involving Na- and Cl-species given in Table 1. The equilibrium constants involving aqueous species were calculated using the revised Helgeson–Kirkham–Flowers (HKF) equations of state (Shock and Helgeson, 1988, 1990; Shock et al., 1989, 1997; Sverjensky et al., 1997, 2014) for the standard partial molal Gibbs free energies of the individual species. The calculations made use of the revised predictive correlation for the equation of state coefficient a_1 in the HKF equations and the new equation of state for the dielectric constant of water that enables calculations at high pressures (Facq et al., 2014, Sverjensky et al., 2014). The thermodynamic properties of aragonite and calcite used below are identical to those we used previously.

Aqueous activity coefficients for the *jth* ion (γ_j) were calculated as in our previous study using the extended Debye–Hückel equation (Helgeson et al., 1981) according to

$$\log\gamma_j = -\frac{A_\gamma Z_j^2 \bar{I}^{0.5}}{1 + a_k^0 B_\gamma \bar{I}^{0.5}} + b_{\gamma,k}\bar{I} + \Gamma_\gamma \quad (1)$$

where A_γ and B_γ represent the Debye–Hückel coefficients calculated from the properties of pure water (Table 1); $\bar{I}$ represents the true ionic strength (corrected for complexing) and a_k^0 and $b_{\gamma,k}$ represent the ion size parameter and the extended term coefficient of the k^{th} electrolyte, respectively. The latter is a function of temperature and pressure (Table 1). Eq. (1) has been shown to apply over very wide ranges of ionic strength in systems in which the solute is dominated by a single electrolyte (Helgeson et al., 1981). The parameter Γ_γ in Eq. (1) represents a conversion from the mole fraction to the molality concentration scale (Helgeson et al., 1981) according to

$$\Gamma_\gamma = \log(1 + 0.0180153 m*) \quad (2)$$

where m^* is equal to the sum of the molalities of all solute species. The value of Γ_γ becomes significant in Eq. (1) at ionic strengths greater than about three. For example, in a 1.0 m NaCl solution without any ion association $\Gamma_\gamma = 0.015$, but in 3.0 and 5.0 m solutions it is 0.03 and 0.07, respectively, which significantly affects the ionic strength dependence of the activity coefficients.

Values of A_γ and B_γ for use in Eq. (1) were calculated from the dielectric constant and density of water using the DEW model

Table 1
Equilibrium constants and extended Debye–Hückel parameters used to calculate model aqueous speciation and aragonite solubilities in NaCl solutions. Equilibrium constants for $Na(HCO_3)^0_{(aq)}$ obtained in the present study by regression of the Raman speciation data at 300 °C are marked with an asterisk. All other values of the equilibrium constants listed were calculated with equations of state for the aqueous species based on fits to published experimental data (Appendix A). Equilibrium constants for the six additional reactions needed to compute the speciation and solubility model of aragonite in water were published previously (Facq et al., 2014).

T (°C)	P (kbar)	$\log K_{Na(HCO_3)^0}$	$\log K_{NaOH^0}$	$\log K_{NaCl^0}$	$\log K_{HCl^0}$	$\log K_{CaCl^+}$	$\log K_{CaCl^0_{2,aq}}$	$\log K_{HSiO_3^-}$	A_a	B_b	A_γ
300	20	−7.3	8.20	0.88	0.26	−0.31	1.00	5.57	0.46	0.34	0.23
	30	−6.2*	7.78	1.08	0.44	−0.09	1.28	4.54	0.41	0.34	0.29
	40	−5.1*	7.43	1.24	0.59	0.06	1.45	3.62	0.37	0.33	0.35
	50	−4.2*	7.14	1.37	0.73	0.18	1.55	2.78	0.34	0.33	0.40
350	20	−7.7	7.88	0.82	−0.01	−0.59	0.73	5.67	0.48	0.35	0.21
	30	−6.6	7.48	1.03	0.18	−0.35	1.06	4.69	0.42	0.34	0.26
	40	−5.6	7.14	1.20	0.33	−0.18	1.26	3.82	0.38	0.33	0.31
	50	−4.7	6.86	1.33	0.47	−0.06	1.39	3.03	0.36	0.33	0.35
	60	−3.9	6.61	1.45	0.60	0.02	1.46	2.29	0.35	0.33	0.39
400	20	−8.1	7.61	0.75	−0.30	−0.86	0.43	5.79	0.51	0.35	0.19
	30	−7.0	7.22	0.98	−0.10	−0.60	0.81	4.85	0.44	0.34	0.23
	40	−6.0	6.90	1.15	0.06	−0.43	1.05	4.02	0.40	0.34	0.27
	50	−5.2	6.62	1.29	0.20	−0.30	1.20	3.27	0.37	0.33	0.30
	60	−4.4	6.38	1.41	0.32	−0.21	1.46	2.57	0.35	0.33	0.33

$\log K_{Na(HCO_3)^0_{aq}}$, $Na(HCO_3)^0_{aq} = Na^+ + H^+ + CO_3^{2-}$; $\log K_{NaOH^0}$, $NaOH^0 + H^+ = Na^+ + H_2O$; $\log K_{NaCl^0}$, $NaCl^0 = Na^+ + Cl^-$; $\log K_{HCl^0}$, $HCl^0 = H^+ + Cl^-$; $\log K_{CaCl^+}$, $CaCl^+ = Ca^{2+} + 2Cl^-$; $\log K_{HSiO_3}$, $HSiO_3^- + H^+ = SiO_2^0 + H_2O$
a. $kg^{0.5}\cdot mol^{-0.5}$; b. $*10^{-8}\cdot kg^{0.5}\cdot mol^{-0.5}$; c. $*10^2$.

(Sverjensky et al., 2014). As in our previous study, the value of a_k^0 was taken equal to that of NaCl, which results in negligible uncertainties at high temperatures and pressures (Manning, 2014). Owing to the paucity of solubility data at elevated pressures and temperatures, as a first approximation, we used the same values of $b_{\gamma,k}$ as in our previous study. The maximum ionic strengths we encountered previously for the aragonite–water system were about 0.4, whereas in the present study of the aragonite–water–NaCl system our experimental data extend to NaCl concentrations of 1.0 m, which corresponds to maximum ionic strengths at the highest pressures studied of about 1.3. Preliminary calculations indicated that the relative concentrations of total dissolved carbonate and bicarbonate are insensitive to the value of $b_{\gamma,k}$ in Eq. (1). Instead, the parameter $b_{\gamma,k}$ does affect calculated solubilities. A test of the applicability of Eq. (1) is described below for the solubility of calcite in NaCl solutions for comparison with experimental data (Newton and Manning, 2002; see also Fig. A3 in Facq et al., 2014). The activity coefficients of neutral species, including the solvent H_2O, were set equal to unity. All the speciation solubility calculations were carried out with the computer code EQ3 (Wolery, 1983) and a custom-built data file containing equilibrium constants calculated with the DEW model as described in Sverjensky et al. (2014) and Facq et al. (2014).

3. Results

3.1. Raman spectroscopic results for carbon speciation in NaCl solutions in equilibrium with aragonite

As previously observed during the dissolution of calcium carbonate in pure water at high pressure and high temperature (Facq et al., 2014), Raman spectra collected in a 0.55 *m* and 1 *m* NaCl aqueous solution in equilibrium with aragonite at 300 °C contain two Raman bands located at 999.5 (4) cm^{-1} and 1062.1 (11) cm^{-1} (Fig. 1). These bands, which correspond respectively to the ν_5 C–OH stretching mode of bicarbonate ions (Frantz, 1998) and the ν_1 symmetric stretching mode of carbonate ions (Oliver & Davis, 1973), become more intense as pressure increases. Carbonate and bicarbonate ions, which may include Ca-complexes of these species, were the only C-bearing species detected by Raman spectroscopy in the aqueous fluid at the total dissolved carbon concentrations of these studies.

The ν_3(E′) and ν_4(E′) vibrational modes of carbonate ions occurring at 1436 cm^{-1} and 684 cm^{-1} respectively (Frantz, 1998), the ν_7(A′), ν_6(A′), ν_4(A′) and ν_3(A′) vibrational modes of bicarbonate ions located at 632, 672, 1302 and 1360 cm^{-1} respectively (Frantz, 1998) as well as those characteristic of the presence of dissolved carbon dioxide (ν_2, ν_3 and ν_4 located at 880, 1395 and 686 cm^{-1} respectively) were not intense enough to be detected by Raman. This could be explained by the relatively low concentrations of total dissolved carbon encountered in the experimental conditions of the present study and by the presence of the very strong and broad T_{2g} vibrational mode of diamond located at 1332 cm^{-1} at ambient pressure and temperature (Huang et al., 2010) which might interfere with the Raman bands of CO_2.

The calcite–aragonite phase transition was marked by the complete dissolution of the calcite crystal and concomitant growth of a euhedral, single crystal of aragonite, as well as the shift of at least −7 cm^{-1} of the ν_1 symmetric stretching mode of carbonate in the crystal. It can be seen in Fig. 2 that the phase transition from calcite to aragonite progressively shifted towards higher pressures with salinity, from 20 kbar in water to 30 kbar in 1.0 m NaCl solutions. Because the exposure time of the calcite crystals to high pressures was similar in all the experiments, the effect of salinity appears to enhance the metastable persistence of calcite.

The relative amounts of the carbonate and bicarbonate ions were estimated from the relative areas of the respective Raman bands mentioned above, after correction from their Raman cross-section as proposed by Frantz (1998). Fig. 2 illustrates the resulting proportions of total dissolved carbonate and bicarbonate as a function of pressure

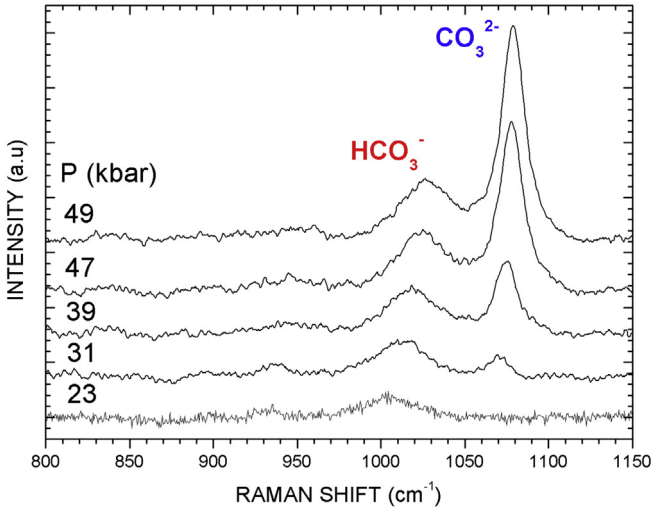

Fig. 1. Evolution of the Raman spectra in a 1 *m* NaCl aqueous fluid at equilibrium with aragonite during its dissolution as a function of pressure at 300 °C.

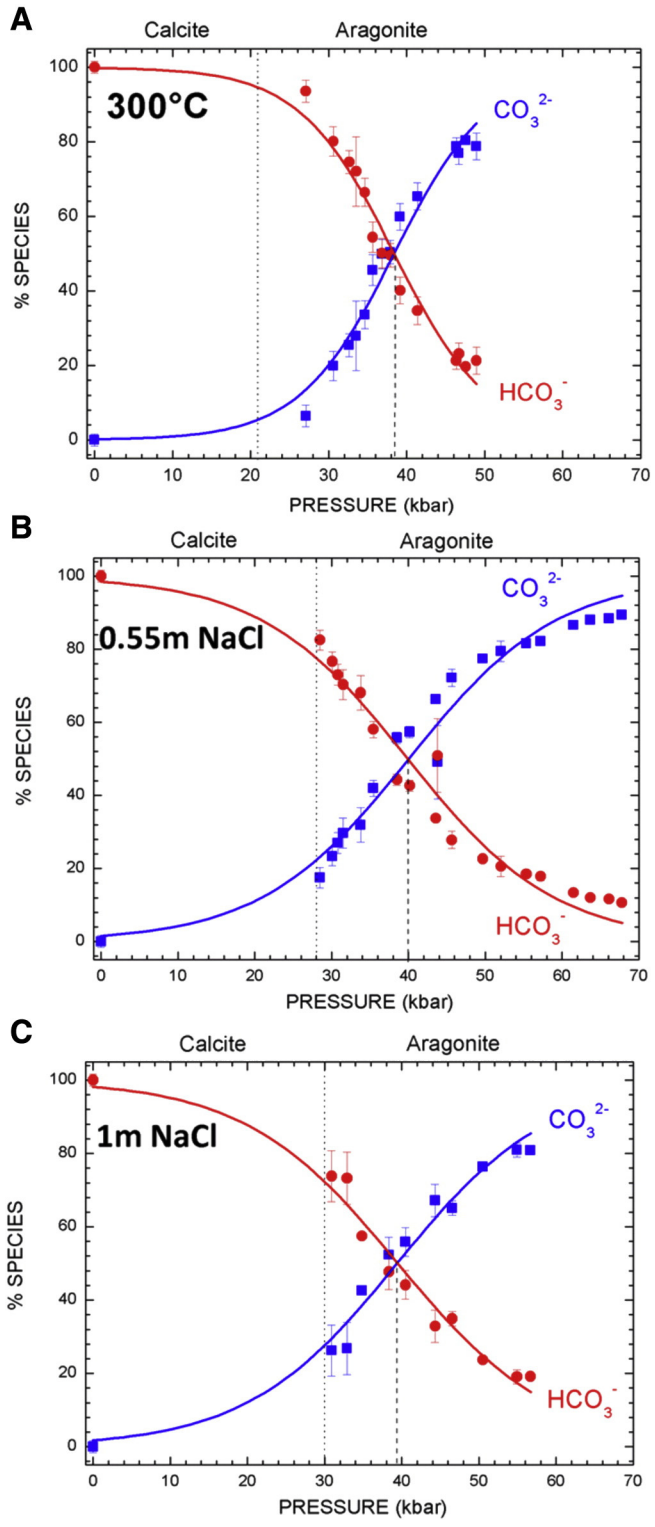

Fig. 2. Pressure dependence of the relative amounts of dissolved total carbonate (blue) and bicarbonate (red) in equilibrium with a crystal of aragonite at 300 °C: (A) Pure water (Facq et al., 2014); (B) 0.55 *m* NaCl solution; (C) 1.0 *m* NaCl solution. Dotted lines locate the calcite–aragonite transition as observed during the experiments. Dashed lines show the pressure at which carbonates and bicarbonates reach equimolality. (For interpretation of the references to colors in this figure legend, the reader is referred to the web version of this article.)

for experiments conducted at 300 °C in aqueous solutions of 0, 0.55 m, and 1.0 m NaCl upon compression and decompression. The solid curves in Fig. 2 represent an empirical sigmoidal fit to the carbonate–bicarbonate speciation as deduced from Raman spectroscopy. This

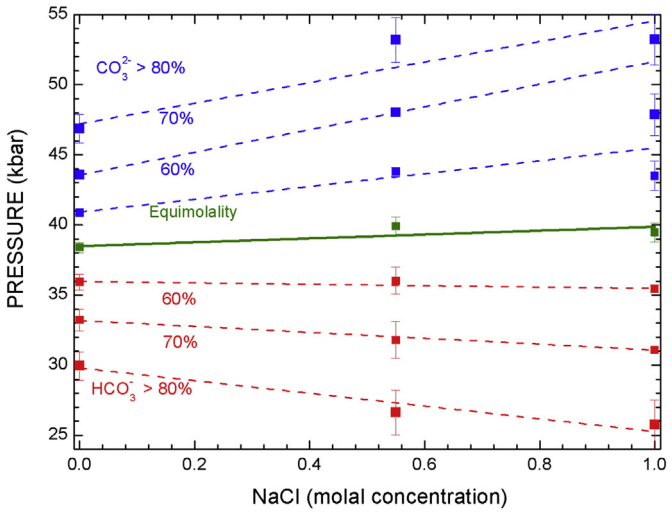

Fig. 3. Distribution of dissolved carbonates and bicarbonates at 300 °C as a function of the fluid salinity. The green curve shows the pressure of equimolality between carbonate and bicarbonate species. Dashed lines represent isopleths where carbonate (blue) and bicarbonate (red) represent more than 60, 70 and 80%, respectively, of the dissolved species. Between those domains, the composition of the fluid is highly variable and this expands as the salinity of the fluid increases. (For interpretation of the references to colors in this figure legend, the reader is referred to the web version of this article.)

enabled calculation of the pressure of equimolality as 39 ± 1 kbar. It can be seen in Fig. 3 that this is constant over the salinity range investigated in the present study. The empirical fit also allowed calculation of isopleths of the relative total amounts of dissolved carbonate and bicarbonate (Fig. 3). For example, along a high-pressure isobar, for instance 47 kbar, the relative amount of bicarbonate increased from 20 to 32% as the salinity increased from 0 to 1.0 m NaCl. Along a lower pressure isobar, *e.g.* 30 kbar, the relative amount of carbonate increased from *ca.* 20 to 28% over the same salinity range.

3.2. Theoretical aqueous speciation and solubility model of aragonite in NaCl solutions

3.2.1. Possible causes of the increased bicarbonate with increasing salinity

As a first step, the previously published model for the speciation and solubility of aragonite in pure water (Facq et al., 2014) was compared with the new Raman data at 1.0 m NaCl. As expected, based on the results above, the model systematically under-predicted the amount of bicarbonate at 40 to 60 kbar in the presence of NaCl. For example, the discrepancies ranged from about 5% too low to about 15% too low at 40 and 50 kbar, respectively. The low bicarbonate predicted by the model could, in principle, arise from an inadequate treatment of aqueous ionic activity coefficients or from the existence of new complexes in the NaCl-system which were not considered in the pure water–aragonite system. However, preliminary calculations varying the aqueous ionic activity coefficients by varying the extended term parameter $b_{\gamma,k}$ (Eq. (1)) by a factor of two did not significantly affect the proportion of bicarbonate to carbonate. This is explained by the form of the mass action expression used in our activity coefficient model (see Facq et al., 2014; Sverjensky et al., 2014). In our model, the activity coefficients of the bicarbonate and proton cancel in the mass action expression, leaving the only activity coefficient of the carbonate ion, which does not change much with ionic strength. For example, as a result of the change from pure water to 1.0 *m* NaCl, the value of $\gamma_{CO_3^{2-}}$ only changes from 0.7 to 0.5. Consequently, the measured change in the bicarbonate–carbonate speciation with increasing NaCl concentration at high pressures is not likely to be attributable to aqueous activity coefficient effects, as the ratio of carbonate to bicarbonate is not sensitive enough to activity coefficients.

A much more likely cause of the increased proportion of bicarbonate to carbonate at higher salinities is the appearance of complexes involving Na^+ or Cl^- in the system studied here compared with the aragonite–water system. Based on previous studies of hydrothermal complexing at lower pressures (Sverjensky et al., 1991, 1997; Stefánsson et al., 2013), new complexes likely to form in our system include those in the following reactions:

$$NaHCO_3^0 = Na^+ + H^+ + CO_3^{2-} \quad (3)$$

$$NaCO_3^- = Na^+ + CO_3^{2-} \quad (4)$$

$$CaCl^+ = Ca^{2+} + Cl^- \quad (5)$$

$$CaCl_2^0 = Ca^{2+} + 2Cl^- \quad (6)$$

$$NaOH^0 = Na^+ + OH^- \quad (7)$$

$$HCl^0 = H^+ + Cl^- \quad (8)$$

$$NaCl^0 = Na^+ + Cl^-. \quad (9)$$

Clearly, the reaction in Eq. (3) forming the complex $NaHCO_3^0$ could potentially be important in enhancing the proportion of bicarbonate to carbonate in equilibrium with aragonite in the NaCl-bearing system whereas, the reaction forming the $NaCO_3^-$ complex in Eq. (4) would have the opposite effect. The other complexes in Eqs. (5) through (9) don't involve carbon, but could conceivably affect the model speciation of bicarbonate and carbonate indirectly to some extent. All the above complexes have been reported in studies at ambient conditions, and some at higher temperatures, but little is known experimentally about these complexes at the conditions of our study. The question for the present study is which complexes might be playing an important role at the novel pressure conditions we have investigated experimentally.

3.2.2. The relative roles of aqueous complexes involving Na and Cl

Equilibrium constants for the complexes in Eqs. (3)–(9) as functions of temperature and pressure have been reported in a variety of studies. Equilibrium constants for $NaHCO_3^0$ and $NaCO_3^-$ extending up to 200 °C have been established (Stefánsson et al., 2013) and the speciation in Na_2CO_3 and $NaHCO_3$ solutions have been studied in the hydrothermal diamond anvil cell to 600 °C and 15 kbar (Schmidt, 2014). For the Ca–Cl complexes, equilibrium constants have been reported up to 325 °C for $CaCl^+$ (Gillespie et al., 1992) and 360 °C for the $CaCl_2^0$ complex (Williams-Jones and Seward, 1989). However, data for these species as a function of pressure are sparse and based on simplistic speciation assumptions. For example, a study of calcsilicate solubilities assumed only $CaCl_2^0$ at 2 kbar (Luce et al., 1985). The results are also inconsistent with each other, *e.g.* the equilibrium constants for $CaCl_2^0$ at 1–4 kbar (Frantz and Marshall, 1982) are inconsistent with the results of Luce et al. (1985). These differences likely arise in part because these studies were based on unreliable values of the dissociation constant of HCl (Sverjensky et al., 1991). Fortunately, new, more precise conductance-based experimental values of the equilibrium constants are now available for the HCl, NaCl and NaOH complexes at pressures to 4 kbar (Ho et al., 1994; Ho and Palmer, 1996; Tagirov et al., 1997; Ho et al., 2001), which greatly helps the analysis of the relative importance of the above reactions.

At the same time, we now also have newly revised predictive methods for calculating the standard partial molal Gibbs free energies of aqueous complexes that can be calibrated with the existing equilibrium constant data as functions of temperature and pressure using the DEW model. Using this approach, we retrieved the standard partial molal entropies, volumes and heat capacities at 25 °C and 1 bar and the equation of state coefficients for the complexes in Eqs. (4)–(9) as discussed in Appendix A and summarized in Table 2. Equilibrium constants for the $NaHCO_3^0$ complex in Eq. (3) are discussed separately below. It should be emphasized that the standard partial molal entropies, volumes and heat capacities at 25 °C and 1 bar are linked to the equation of state coefficients of each species by the revised predictive correlations described in Sverjensky et al. (2014) and Facq et al. (2014) which are built into the DEW model. Values of the equilibrium constants used in this study are given in Table 1.

A preliminary assessment of the likely relative importance of these complexes for aragonite in equilibrium with 1.0 *m* NaCl at 300 °C and pressures of up to 50 kbar indicated that the species $NaCO_3^-$, $CaCl_2^0$, NaOH and HCl are of minor importance in our experimental fluids. In addition, the calculations indicated that the proportions of bicarbonate to carbonate were not sensitive to the strengths of the Ca–Cl complexes or the NaCl complex. Instead, as expected, the model proportions of total bicarbonate to total carbonate were very sensitive to the strength

Table 2
Equation of state coefficients for use in the revised HKF equations of state for aqueous species consistent with the equilibrium constants given in Table 1 and Appendix A. The partial molal properties and equation of state coefficients for $Na(HCO_3)^0$ were obtained in the present study by regression of the equilibrium constants given in Table 1 and Fig. 5 (see text). The partial molal properties and the equation of state coefficients for all the other aqueous species were obtained by regression of published experimental data (Appendix A) or as indicated. All equation of state parameters were computed using correlations with the partial molal properties (Shock and Helgeson, 1988; Shock et al., 1989; Sverjensky et al., 2014) unless otherwise noted.

SPECIES	ΔG_f^0 [a]	ΔH_f^0 [a]	S^0 [b]	C_P^0 [b]	V^0 [c]	a_1 [d]	a_2 [a]	a_3 [e]	a_4 [f]	c_1 [b]	c_2 [f]	ω [a]
$NaHCO_3^0$	−203,088[g]	−224,487.[h]	31.0[g]	74.0[g]	36.7[j]	9.61	2.56	1.01	−2.88	55.5	12.0	0.65[j]
$NaCO_3^-$	−190,562.	−209,097.[h]	8.0[i]	−1.0[i]	27.8	7.64	2.99	2.33	−2.90	19.47	−3.24	1.51
$NaOH^0$	−100,900.	−114,577.[h]	6.5	42.0	12.0	3.95	−0.53	5.28	−2.76	32.6	5.52	0.20
$NaCl^0$	−92,910.	−96,120.[h]	28.0	8.5	24.0	6.16	1.58	3.51	−2.84	10.8	−1.30	−0.038
HCl^0	−30,410.	−32,056.[h]	3.2	39.0	15.0	4.34	−0.15	4.97	−2.77	27.2	4.91	−0.20
$CaCl^+$	−163,100.	−177,310.[h]	4.5	17.5	11.3	3.94	−0.53	5.28	−2.76	20.7	0.53	0.47
$CaCl_2^0$	−194,000.	−211,051.[h]	6.0	29.8	33.3	7.97	3.30	2.07	−2.92	23.3	3.03	−0.038
$HSiO_3^-$	−242,855.	−266,717.[h]	−2.0[l]	10.5[l]	18.2[l]	5.85	1.29	3.76	−2.83	27.61	−0.90	1.6594

[a] $cal \cdot mol^{-1}$.
[b] $cal \cdot mol^{-1} \cdot K^{-1}$.
[c] $cm^{-3} \cdot mol^{-1}$.
[d] $cal \cdot mol^{-1} \cdot bar^{-1}$.
[e] $cal \cdot K \cdot mol^{-1} \cdot bar^{-1}$.
[f] $cal \cdot K \cdot mol^{-1}$.
[g] Retrieved by regression of experimental equilibrium constants shown in Fig. 5 at $P_{sat.}$ (see text).
[h] Calculated from the given values of ΔG_f^0 and S^0 and the third law entropies of the elements from Helgeson et al. (1978).
[i] Retrieved by regression of experimental equilibrium constants from Stefánsson et al. (2013) and Garrels et al. (1961).
[j] Retrieved from fitting the equilibrium constants referring to pressures of 30, 40, and 50 kbar (Fig. 5; Table 1).

of the $NaHCO_3^0$ complex. The presence of this complex in large enough amounts can easily account for the enhancement of total bicarbonate relative to total carbonate observed in the Raman experiments with saline solutions compared with the aragonite–water system.

It should be noted that if our predicted $NaCO_3^-$ complex is in error and should in fact be more abundant than we predict, too much total carbonate relative to total bicarbonate would be predicted by the speciation model, which is inconsistent with the Raman data. This could be offset by increasing the strength of the predicted $NaHCO_3^0$ complex in order to obtain consistency with the Raman data. Overall, regardless of the true strength of the $NaCO_3^-$ complex, the Raman speciation results require a significant role for the $NaHCO_3^0$ complex. In the absence of independent experimental equilibrium constants for the $NaHCO_3^0$ and $NaCO_3^-$ complexes at high pressures, we adopted the simplest approximation: we assumed that the $NaHCO_3^0$ complex accounts for all of the enhancement of bicarbonate relative to carbonate observed in the Raman data at the higher salinities.

3.2.3. Regression of the Raman speciation data to quantify the $NaHCO_3^0$ complex

Based on the assumption that the $NaHCO_3^0$ complex accounts for the enhancement of bicarbonate relative to carbonate in 0.55 and 1.0 m NaCl solutions in equilibrium with aragonite, we used the Raman speciation to retrieve new values of the equilibrium constant of $NaHCO_3^0$ under the experimental conditions from 30 to 50 kbar. The values are reported in Table 1. These new equilibrium constants at high pressures were used together with published equilibrium constants at lower pressures and temperatures to derive a revised equation of state characterization of $NaHCO_3^0$ that enables predictions under conditions far removed from the experimental pressures and temperatures (see below).

Our final fits to the Raman speciation data for 0, 0.55 and 1.0 *m* NaCl are represented by the solid curves shown in Fig. 4A–C. The model of C-speciation is shown in Fig. 4D–F, and the model of Ca-speciation is shown in Fig. 4G–I. The figures representing aragonite in water (Facq et al., 2014) are shown for comparative purposes. It can be seen in

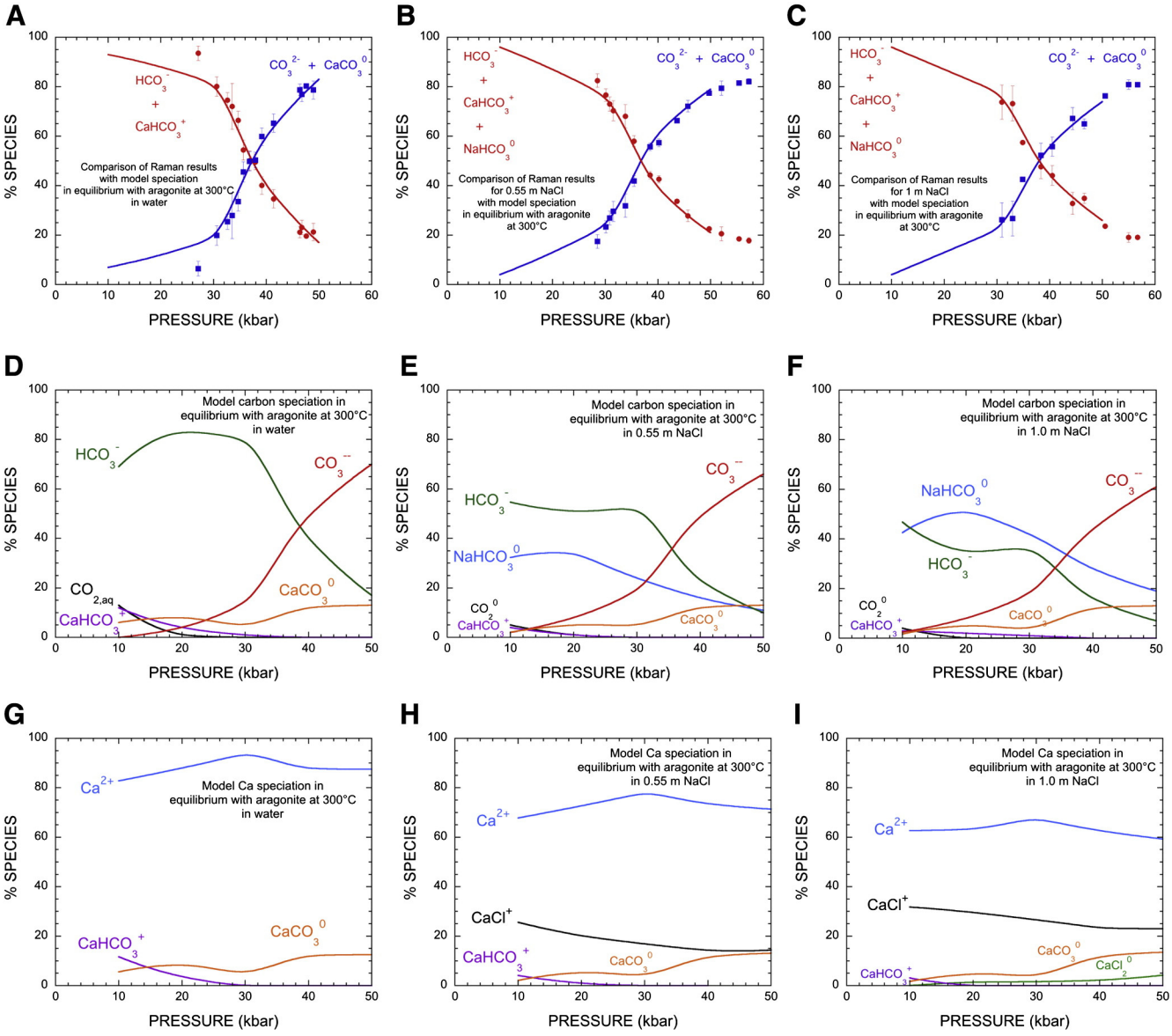

Fig. 4. Theoretically calculated curves from a speciation–solubility model of aragonite in equilibrium with NaCl solutions at 300 °C: (A) In water, (B) 0.55 m NaCl; and (C) 1.0 m NaCl. The curves were constrained to fit the Raman speciation data in (B) and (C) by retrieving the equilibrium constant for the complex $NaHCO_3^0$ (Table 1) using the equation of state parameters for the aqueous species given in Table 2 and in Facq et al. (2014). The model C-speciation changes with pressure are shown in (D)–(F), and the model Ca–speciation changes with pressure are shown in (H)–(J).
Data from (A), (D), and (G) are from Facq et al. (2014).

Fig. 4B and C that the regression curves for both the 0.55 and 1.0 *m* NaCl solutions closely fit the experimental data with a single value for the equilibrium constant for $NaHCO_3^0$ at each pressure from 30 to 50 kbar (Table 1). It should be emphasized that all our previously published equilibrium constants for the aragonite–water system were also used in these calculations, together with the values of $b_{\gamma,k}$ published previously, and the newly predicted equilibrium constants in Table 1. Only, the equilibrium constant for the $NaHCO_3^0$ complex was obtained by regression at 300 °C and pressures of 30, 40 and 50 kbar (Table 1).

The model speciation of C and Ca shown in Fig. 4D–I reveal clear trends with increasing salinity. Most notable for the C-speciation is the increase in the relative abundance of the $NaHCO_3^0$ complex at a given pressure with increased salinity (Fig. 4D–F). The enhanced formation of this species can be thought of as consuming protons, raising the pH and increasing the solubility because more Na^+ ions complex more HCO_3^-. In contrast, at a given salinity (*e.g.* Fig. 4F), increasing pressure from about 20 to 50 kbar causes dissociation of the $NaHCO_3^0$ complex which reduces the pH and simultaneously enhances the solubility. In this instance, the solubility increase with pressure occurs despite the dissociation of the $NaHCO_3^0$ complex. The reason for this is a change of speciation. With increasing pressure, there is a dramatic increase in the abundance of the carbonate ion, which causes the simple solubility product of aragonite (*i.e.* in terms of Ca^{2+} and CO_3^{2-} ions) to be the major control on solubility, and the equilibrium constant for that reaction increases strongly with pressure (Facq et al., 2014, Fig. 7A), which in turn increases the solubility.

4. Discussion

4.1. Aqueous carbon complexing at high temperatures and pressures

4.1.1. Carbon speciation in Na-bearing solutions

Our experimental data for aqueous carbon speciation in equilibrium with aragonite at 40–60 bar and 300 °C clearly showed more bicarbonate and less carbonate as the salt concentration increased. This change constrained the development of an aqueous speciation–solubility model of aragonite in NaCl solutions. Our theoretical model developed above was used to interpret the increase in the proportion of the total bicarbonate to total carbonate with salinity in terms of the formation of a $NaHCO_3^0$ aqueous complex.

It should be noted that Na-bicarbonate or Na-carbonate complexes cannot be detected by Raman spectroscopy at the relatively low concentrations of dissolved carbon imposed by the solubility of aragonite in our current experiments. In aqueous solutions without a Ca-carbonate mineral present, much higher initial carbonate or bicarbonate concentrations can be achieved. For example, a $NaCO_3^-$ complex was reported in 1.6 m Na_2CO_3 solutions at temperatures greater than 400 °C and pressures up to 1.5 kbar (Schmidt, 2014). The relative concentrations of the three species HCO_3^-, CO_3^{2-} and $NaCO_3^-$ were obtained by fitting three components to two asymmetric Raman peaks (Schmidt, 2014). However, in the same study, a $NaHCO_3^0$ complex was not detected even in a 4.6 m $NaHCO_3$ solution at elevated temperatures and pressures up to 600 °C and 0.15 kbar. In contrast, a combined potentiometric and ultraviolet spectroscopic study of solutions in the Na_2O–CO_2–H_2O–HCl system (Stefánsson et al., 2013) has reported the characterization of equilibrium constants for both the $NaCO_3^-$ and $NaHCO_3^0$ complexes to temperatures of 200 °C at $P_{sat.}$ pressures.

Our thermodynamic model integrates both low and high temperature and pressure data for solubility and speciation in the CaO–CO_2–H_2O–HCl–NaCl system. Using our equation of state approach for aqueous species enables us to integrate the equilibrium constants from Stefánsson et al. (2013), as well as the results from previous studies at low temperatures and pressures, with the equilibrium constants for the $NaHCO_3^0$ complex retrieved from the Raman data as described above. Our model is not applicable to the bicarbonate to carbonate concentration ratios obtained by Schmidt (2014) because the fluids in those experiments are likely to be extremely alkaline as well as very high in ionic strength. Furthermore, the concentration ratios of the aqueous species obtained by Schmidt (2014) were based on assumptions for the ratios of the scattering factors different to those adopted in Facq et al. (2014).

Our focus is on the geologically important fluids in which Ca-carbonate minerals constrain the solubility and aqueous speciation of carbon at the elevated pressures and temperatures characteristic of subduction zone conditions. Although our experimental Raman results presented above refer only to 300 °C, they do refer to very high pressures not previously studied for carbonate mineral solubilities in NaCl solutions, and, importantly, the experimental results can be extrapolated to much higher temperatures using our thermodynamic model. In order to do this, we develop below an equation of state representation of the $NaHCO_3^0$ complex.

4.1.2. Equation of state characterization of aqueous $NaHCO_3^0$

Values of the equilibrium constant of $NaHCO_3^0$ derived from fitting the Raman speciation data at high pressures together with data from the literature at lower pressures and temperatures are shown in Fig. 5. The solid curves represent regression of the experimental data using the methods described in Sverjensky et al. (1997). In this approach, the combined data set of low and high temperature/pressure experimental data are used to retrieve five parameters: the standard partial molal Gibbs free energy of formation, the standard partial molal entropy, volume and heat capacity of the complex at 25 °C and 1 bar, and the value of the equation of state parameter Ω by assuming that these quantities are linked by established correlations to the remaining equation of state coefficients of the $NaHCO_3^0$ complex. Here we use the revised predictive correlations described in Sverjensky et al. (2014) and Facq et al. (2014) that are built into the DEW model as a guide to determining the equation of state coefficients.

With the above approach, the low pressure data along the $P_{sat.}$ curve (Nakayama, 1971; Stefánsson et al., 2013) enabled retrieval of the values of the standard partial molal free energy, entropy and heat capacity of $NaHCO_3^0$. The data at high pressures enabled retrieval of the values of the standard partial volume and the equation of state coefficient Ω for $NaHCO_3^0$. The values of all the standard partial

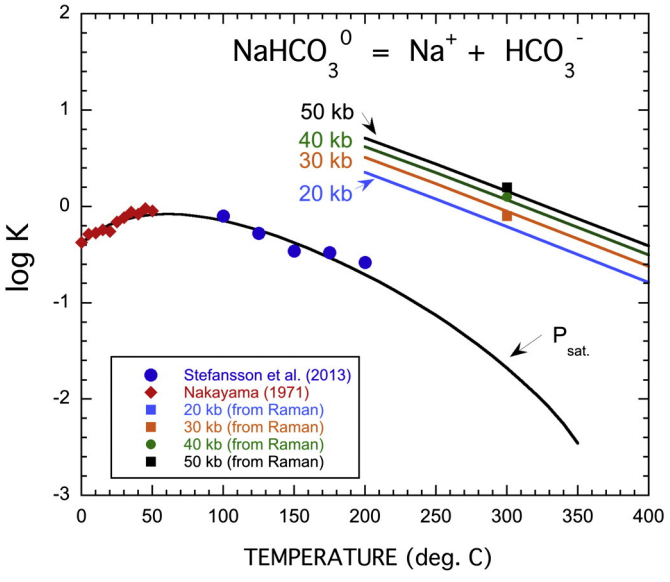

Fig. 5. Values of the logarithm of the equilibrium constant for the complex $NaHCO_3^0$ as functions of temperature and pressure. The solid squares were retrieved from fitting the Raman speciation data (Table 1). The other symbols represent data from the literature. The solid curves represent a fit to all of the data to constrain the standard partial molal properties and equation of state coefficients for the complex $NaHCO_3^0$ based on the properties of the Na^+ and HCO_3^- ions.

molal properties and the other equation of state coefficients are given in Table 2.

Of the coefficients influencing the behavior of the species with pressure, the coefficient a_1 is by far the most important. Here the value of a_1 was obtained from a correlation with the value of the volume retrieved from the trend of the high-pressure equilibrium constants. It can be seen in Table 2 that the value of $10\times a_1$ obtained is equal to 9.6 cal·mol^{-1} bar^{-1}. This is very close to the sum of the $10\times a_1$ values of the Na^+ and the HCO_3^- ions (9.5 cal·mol^{-1} bar^{-1}), a result typical of many inorganic aqueous metal species (Sverjensky et al., 2014). Similarly, a value of $10^5 \times \Omega$ is equal to 0.65 cal·mol^{-1}, which is reasonably close to 0.3 ($\pm$0.2) cal·mol^{-1} typical of many neutral inorganic and organic aqueous species (*e.g.* Plyasunov and Shock, 2001; Sverjensky et al., 2014).

These results provide a strong indication that our equation of state characterization of the $NaHCO_3^0$ complex is consistent with the results for a wide variety of other aqueous species. In turn, this suggests that we can use our equation of state coefficients for $NaHCO_3^0$ to make predictions of the dissociation constant at pressures and temperatures where there are no experimental data. A test of this assertion is described next.

4.1.3. Model testing using the solubility of calcite in NaCl solutions at high temperatures and pressures

Measurements of the solubilities of carbonate minerals in salt solutions at elevated pressures are sparse (Fein and Walther, 1989; Newton and Manning, 2002). Of these studies, the highest-pressure results refer to the solubility of calcite in NaCl solutions reported at 10 kbar and 600–900 °C by Newton and Manning (2002). These data cover a very wide range of NaCl concentrations to more than 20 *m* NaCl, which is much higher than we can reasonably expect our solubility–speciation model to apply. There are two main reasons for this. One is that Eq. (1) alone may not be adequate to account for the high ionic strengths in such solutions that actually represent mixed electrolytes because of the tremendous solubility enhancement at high salt concentrations. A second reason is that at very high levels of NaCl, it is possible that additional aqueous complexes that we have not considered may become important. Nevertheless, the data at the lowest NaCl concentrations (all of which are greater than 1.0 *m* NaCl) serve as a test of the overall approach taken in the present study.

Experimental solubility data from Newton and Manning (2002) at 10 kbar and 700 °C are shown in Fig. 6A together with the calculated solubility of calcite as a function of NaCl concentration predicted using the model described above with a range of $b_{\gamma,k}$ values. The calculated curves represent a test of the predicted equilibrium constants of all the species. It can be seen in Fig. 6A that with $b_{\gamma,k} = -0.05$, the overall trend of the calculated curve is very reasonable up to quite high salinities. The value of $b_{\gamma,k} = -0.05$ would be expected to be less than the values in Table 1 because Fig. 6A refers to much higher temperatures than the experimental conditions in the table. Previous estimations of the behavior of values of $b_{\gamma,k}$, with temperature (Helgeson et al., 1981) indicate a strong decrease of values of $b_{\gamma,k}$, with temperature.

It can be seen in Fig. 6B that with $b_{\gamma,k} = -0.05$ at 700 °C and 10 kbar more than 99% of the total model C-solubility consists of the species CO_2, $Ca(HCO_3)^+$ and $NaHCO_3^0$. The high abundance of the neutral species CO_2 in Fig. 6B compared with the very low abundance in Fig 4D–F indicates the strong effect of temperature on the speciation of carbon. Furthermore, the high abundance of neutral species in the model results in a limited sensitivity of the calculated solubilities to the specific value of $b_{\gamma,k}$. Overall, these results provide further support for the applicability of the equilibrium constants and activity coefficient model of the present study to predicting solubilities and aqueous speciation at high temperatures and pressures, as well as NaCl concentrations approaching 10 *m*.

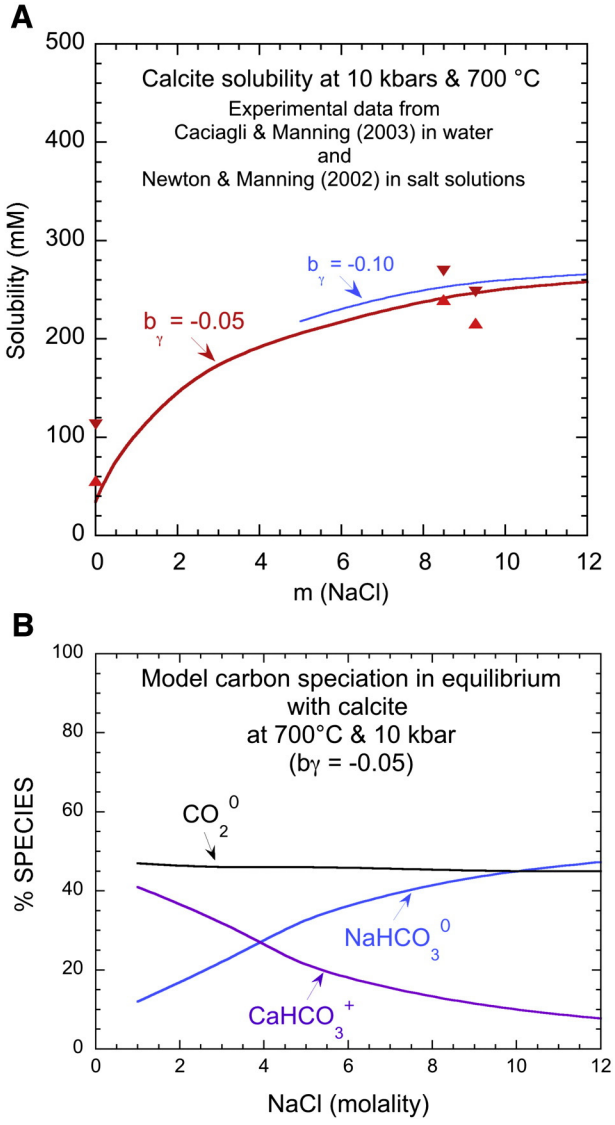

Fig. 6. Calculated solubility of calcite and carbonate speciation as a function of NaCl concentration at 700 °C and 10 kbar. The predictions were made using the solubility and speciation model of the present study, including a predicted value of the equilibrium constant for the complex $NaHCO_3^0$, for comparison with experimental measurements by Newton & Manning (2002): (A) Calculated solubility curves for calcite with a range of different values for the extended Debye–Hückel parameter ($b_{\gamma,k}$); (B) predicted speciation of carbonate in NaCl solutions ($b_{\gamma,k} = -0.05$) in equilibrium with calcite.

5. Conclusions

This study represents an integrated experimental and theoretical effort to address the lack of information about the aqueous speciation and solubility of carbon in NaCl-bearing fluids at high pressures. Specifically, our experiments address fluids in the calcium carbonate–water–salt system at 300 °C to pressures of 70 kbar. Our theoretical model, calibrated in part with our experimental results, enables predictions of carbonate mineral solubility to higher temperatures than in the experiments.

Our experimental study of the carbon speciation during equilibration of aragonite in NaCl solutions at 300 °C from 20 to 70 kbar used *in situ* Raman spectroscopy in a diamond anvil cell with NaCl concentrations up to 1.0 *m* (5.5 wt.%). Bicarbonate and carbonate ions were the only C-bearing aqueous species spectroscopically detected in the fluids. The proportion of total dissolved bicarbonate to carbonate increased with NaCl concentration and was interpreted using a thermodynamic model to retrieve the dissociation constant of the $NaHCO_3^0$ complex. An equation of state approach using the DEW model was used to

integrate our equilibrium constants for the $NaHCO_3^0$ complex with literature data referring to low temperatures and pressures.

In order to facilitate the geologic applicability of our experimental and model results, we used the DEW model to extrapolate equilibrium constants to high temperatures and pressures, which enables prediction of calcite and aragonite solubilities and aqueous speciation in chloride solutions. The model was tested by comparison with the experimental solubilities of calcite in NaCl solutions at 700 °C and 10 kbar from Newton and Manning (2002). This result serves as a model for an aqueous fluid in Ca-carbonate-rich metasedimentary rocks. It suggests that substantial amounts of carbon can be transported as a consequence of the solubility of carbonate rocks in subduction zones at high pressures.

Acknowledgments

The authors are indebted to J. Fein, G. D. Miron, and an anonymous referee for their constructive reviews. We wish to acknowledge the support and collaboration of the 'Reservoirs and Fluxes' and 'Extreme Physics and Chemistry' communities of the Deep Carbon Observatory and support from the NSF EAR-1023865 (DAS), DOE DE-FG02-96ER-14616 (DAS), and NASA Astrobiology Institute (NASA Award 4100674053). The Raman facility at the Ecole Normale Supérieure de Lyon is supported by the Institut National des Sciences de l'Univers (INSU).

Appendix A. Supplementary data

Supplementary data to this article can be found online at http://dx.doi.org/10.1016/j.chemgeo.2016.03.021.

References

Ague, J.J., Nicolescu, S., 2014. Carbon dioxide released from subduction zones by fluid-mediated reactions. Nat. Geosci. 7, 355–360.
Berner, R.A., 2004. The Phanerozoic Carbon Cycle CO_2 and O_2. Oxford University Press, New York.
Caciagli, N.C., Manning, C.E., 2003. The solubility of calcite in water at 6–16 kbar and 500–800 °C. Contrib. Mineral. Petrol. 146, 275–285.
Chervin, J.–.C., Canny, B., Besson, J.–.M., Pruzan, P., 1995. A diamond anvil cell for IR microspectroscopy. Rev. Sci. Instrum. 66, 2595–2598.
Dasgupta, R., 2013. Ingassing, Storage, and Outgassing of Terrestrial Carbon Through Geologic Time. In: Hazen, R.M., Jones, A.P., Baross, J.A. (Eds.), Carbon in Earth. Reviews in Mineralogy & Geochemistry, pp. 183–229.
Dasgupta, R., Hirschmann, M.M., Dellas, N., 2005. The effect of bulk composition on the solidus of carbonated eclogite from partial melting experiments at 3 kbar. Contrib. Mineral. Petrol. 149, 288–305.
Duan, Z.H., Li, D.D., 2008. Coupled phase and aqueous species equilibrium of the H_2O–CO_2–NaCl–$CaCO_3$ system from 0 to 250 °C, 1 to 1000 bar with NaCl concentrations up to saturation of halite. Geochim. Cosmochim. Acta 72, 5128–5145.
Ellis, A.J., 1963. Solubility of calcite in sodium chloride solutions at high temperatures. Am. J. Sci. 261, 259.
Facq, S., Daniel, I., Montagnac, G., Cardon, H., Sverjensky, D.A., 2014. In situ Raman study and thermodynamic model of aqueous carbonate speciation in equilibrium with aragonite under subduction zone conditions. Geochim. Cosmochim. Acta 132, 375–390.
Fein, J.B., Walther, J.V., 1987. Calcite solubility in supercritical CO_2–H_2O fluids. Geochim. Cosmochim. Acta 51, 1665–1673.
Fein, J.B., Walther, J.V., 1989. Calcite solubility and speciation in supercritical NaCl–HCl aqueous fluids. Contrib. Mineral. Petrol. 103, 317–324.
Frantz, J.D., 1998. Raman spectra of carbonate and bicarbonate aqueous fluids at elevated temperatures and pressures: comparison with theoretical calculations. Chem. Geol. 1998, 211–225.
Frantz, J.D., Marshall, W.L., 1982. Electrical conductances and ionization constants of calcium chloride and magnesium chloride in aqueous solutions at temperatures to 600 °C and pressures to 4000 bars. Am. J. Sci. 282, 1666–1693.
Frezzotti, M., Selverstone, J., Sharp, Z., Compagnoni, R., 2011. Carbonate dissolution during subduction revealed by diamond-bearing rocks from the Alps. Nat. Geosci. 4, 703–706.
Garrels, R.M., Thompson, M.E., Siever, R., 1961. Control of carbonate solubility by carbonate complexes. Am. J. Sci. 259, 24–45.
Gillespie, S.E., Oscarson, J.L., Chen, X., Izatt, R.M., Pando, C., 1992. Thermodynamic quantities for the interaction of Cl^- with Mg^{2+}, Ca^{2+} and H^+ in aqueous solution from 250 to 325 °C. J. Solut. Chem. 21, 761–788.
Hacker, B.R., Abers, G.A., Peacock, S.M., 2003a. Subduction factory 1. Theoretical mineralogy, densities, seismic wave speeds, and H_2O contents. J. Geophys. Res. Solid Earth 108 (B1), 2029.
Hacker, B.R., Peacock, S.M., Abers, G.A., Holloway, S.D., 2003b. Subduction factory 2. Are intermediate-depth earthquakes in subducting slabs linked to metamorphic dehydration reactions? J. Geophys. Res. Solid Earth 108 (B1), 2030.
Helgeson, H.C., Kirkham, D.H., Flowers, G.C., 1981. Theoretical prediction of the thermodynamic behavior of aqueous electrolytes at high pressures and temperatures. IV. Calculation of activity coefficients, osmotic coefficient and apparent molal and standard and relative partial molal properties to 600 °C and 5 kbar. Am. J. Sci. 287, 1249–1516.
Helgeson, H.C., Delany, J.M., Nesbitt, H.W., Bird, D.K., 1978. Summary and critique of the thermodynamic properties of rock-forming minerals. Am. J. Sci. 278, 1–229.
Ho, P.C., Palmer, D.A., 1996. Ion association of dilute aqueous sodium hydroxide solutions to 600 degrees C and 300 MPa by conductance measurements. J. Solut. Chem. 25, 711–729.
Ho, P.C., Palmer, D.A., Gruszkiewicz, M.S., 2001. Conductivity measurements of dilute aqueous HCl solutions to high temperatures and pressures using a flow-through cell. J. Phys. Chem. B 105, 1260–1266.
Ho, P.C., Palmer, D.A., Mesmer, R.E., 1994. Electrical-conductivity measurements of aqueous sodium–chloride solutions to 600 °C and 300 MPa. J. Solut. Chem. 23, 997–1018.
Huang, E.–.P., et al., 2010. High-temperature and pressure Raman spectroscopy of diamond. Mater. Lett. 64, 580–582.
Kelemen, P.E., Manning, C., 2015. Reevaluating carbon fluxes in subduction zones, what goes down, mostly comes up. Proc. Natl. Acad. Sci. U. S. A. 112, E3997–E4006.
Kerrick, D.M., Connolly, J.A.D., 1998. Subduction of ophicarbonates and recycling of CO_2 and H_2O. Geology 26, 375–378.
Kerrick, D.M., Connolly, J.A.D., 2001a. Metamorphic devolatilization of subducted marine sediments and the transport of volatiles into the Earth's mantle. Nature 411, 293–296.
Kerrick, D.M., Connolly, J.A.D., 2001b. Metamorphic devolatilization of subducted oceanic metabasalts: implications for seismicity, arc magmatism and volatile recycling. Earth Planet. Sci. Lett. 189, 19–29.
Luce, R., Cygan, G., Hemley, J., D'angelo, W., 1985. Some mineral stability relations in the system CaO–MgO–SiO_2–H_2O–HCl. Geochim. Cosmochim. Acta 49, 525–538.
Malinin, S.D., Kanukov, A.B., 1971. Solubility of calcite in homogeneous H_2O–NaCl–CO_2 systems in 200–600 °C temperature interval. Geochemistry Int$^+$ USSR 8, pp. 668–679.
Manning, C.E., 2014. Geochemistry: a piece of the deep carbon puzzle. Nat. Geosci. 7, 333–334.
Manning, C.E., Shock, E.L., Sverjensky, D.A., 2013. The Chemistry of Carbon in Aqueous Fluids at Crustal and Upper-mantle Conditions: Experimental and Theoretical Constraints. In: Hazen, R.M., Jones, A.P., Baross, J.A. (Eds.), Carbon in Earth. Reviews in Mineralogy & Geochemistry, pp. 109–148.
Martinez, I., Sanchez–Valle, C., Daniel, I., Reynard, B., 2004. High-pressure and high-temperature Raman spectroscopy of carbonate ions in aqueous solution. Chem. Geol. 207, 47–58.
Molina, J.F., Poli, S., 2000. Carbonate stability and fluid composition in subducted oceanic crust: an experimental study on H_2O–CO_2-bearing basalts. Earth Planet. Sci. Lett. 178, 295–310.
Nakayama, F.S., 1971. Thermodynamic functions for the dissociation of $NaHCO_3^0$, $NaCO_3-$, H_2CO_3 and HCO_3^-. J. Inorg. Nucl. Chem. 33, 1287–1291.
Newton, R.C., Manning, C.E., 2002. Experimental determination of calcite solubility in H_2O–NaCl solutions at deep-crust/upper mantle pressures and temperatures: implications for metasomatic processes in shear zones. Am. Mineral. 87, 1401–1409.
Newton, R.C., Manning, C.E., 2005. Solubility of anhydrite, $CaSO_4$, in NaCl–H_2O solutions at high pressures and temperatures: applications to fluid–rock interaction. J. Petrol. 46, 701–716.
Oliver, B.G., Davis, A.R., 1973. Vibrational spectroscopic studies of aqueous alkali metal bicarbonate and carbonate solutions. Can. J. Chem. 51, 698–702.
Plyasunov, A.V., Shock, E.L., 2001. Correlation strategy for determining the parameters of the revised Helgeson–Kirkham–Flowers model for aqueous nonelectrolytes. Geochim. Cosmochim. Acta 65, 3879–3900.
Sanchez–Valle, C., Martinez, I., Daniel, I., Philippot, P., Simionovici, A., 2003. Dissolution of strontianite at upper mantle P–T conditions: an in situ synchrotron X-ray fluorescence study. Am. Mineral. 88, 978–985.
Sano, Y., Williams, S.N., 1996. Fluxes of mantle and subducted carbon along convergent plate boundaries. Geophys. Res. Lett. 23, 2749–2752.
Scambelluri, M., Philippot, P., 2001. Deep fluids in subduction zones. Lithos 55, 213–227.
Schmidt, C., 2014. Raman spectroscopic determination of carbon speciation and quartz solubility in H_2O + Na_2CO_3 and H_2O + $NaHCO_3$ fluids to 600 °C and 1.53 kbar. Geochim. Cosmochim. Acta 145, 281–296.
Shock, E.L., Helgeson, H.C., 1988. Calculation of the thermodynamic and transport properties of aqueous species at high pressures and temperatures: correlation algorithms for ionic species and equation of state predictions to 5 kb and 1000 °C. Geochim. Cosmochim. Acta 52, 2009–2036.
Shock, E.L., Helgeson, H.C., 1990. Calculation of the thermodynamic and transport properties of aqueous species at high pressures and temperatures: standard partial molal properties of organic species. Geochim. Cosmochim. Acta 54, 915–945.
Shock, E.L., Helgeson, H.C., Sverjensky, D.A., 1989. Calculation of the thermodynamic and transport properties of aqueous species at high pressures and temperatures: standard partial molal properties of inorganic neutral species. Geochim. Cosmochim. Acta 53, 2157–2183.
Shock, E.L., Sassani, D.C., Willis, M., Sverjensky, D.A., 1997. Inorganic species in geologic fluids: correlations among standard molal thermodynamic properties of aqueous ions and hydroxide complexes. Geochim. Cosmochim. Acta 61, 907–950.
Stefánsson, A., Bénézeth, P., Schott, J., 2013. Carbonic acid ionization and the stability of sodium bicarbonate and carbonate ion pairs to 200 °C — a potentiometric and spectrophotometric study. Geochim. Cosmochim. Acta 120, 600–611.

Sverjensky, D.A., Harrison, B., Azzolini, D., 2014. Water in the deep Earth: the dielectric constant and the solubilities of quartz and corundum to 60 kb and 1200 °C. Geochim. Cosmochim. Acta 129, 125–145.

Sverjensky, D.A., Hemley, J.J., D'Angelo, W.M., 1991. Thermodynamic assessment of hydrothermal alkali feldspar–mica–aluminosilicate equilibria. Geochim. Cosmochim. Acta 55, 989–1004.

Sverjensky, D.A., Shock, E.L., Helgeson, H.C., 1997. Prediction of the thermodynamic properties of aqueous metal complexes to 1000 °C and 5 kb. Geochim. Cosmochim. Acta 61, 1359–1412.

Tagirov, B.R., Zotov, A.V., Akinfiev, N.N., 1997. Experimental Study of Dissociation of HCl from 350 to 500 °C and from 500 to 2500 bars: Thermodynamic Properties of $HCl^0_{(aq)}$.

Tsuno, K., Dasgupta, R., 2012. The effect of carbonates on near-solidus melting of pelite at 3 kbar: relative efficiency of H_2O and CO_2 subduction. Earth Planet. Sci. Lett. 319, 185–196.

van Keken, P.E., Hacker, B.R., Syracuse, E.M., Abers, G.A., 2011. Subduction factory: 4. Depth-dependent flux of H_2O from subducting slabs worldwide. J. Geophys. Res. Solid Earth 116 (B1), B01401.

Walther, J., Long, M., 1986. Experimental determination of calcite solubilities in supercritical H_2O. Int Symp Water–Rock Interaction, pp. 609–611.

Williams– Jones, A.E., Seward, T.M., 1989. The stability of calcium chloride ion pairs in aqueous solutions at temperatures between 100 and 360 °C. Geochim. Cosmochim. Acta 53, 313–318.

Wolery, T.J., 1983. EQ3NR: A Computer Program for Geochemical Aqueous Speciation–Solubility Calculations, User's Guide and Documentation. UCRL-53414. Lawrence Livermore Lab., Univ. Calif.

Yaxley, G.M., Green, D.H., 1994. Experimental demonstration of refractory carbonate-bearing eclogite and siliceous melt in the subduction regime. Earth Planet. Sci. Lett. 128, 313–325.